

ZELDA, a Zernike wavefront sensor for the fine measurement of quasi-static aberrations in coronagraphic systems: concept studies and results with VLT/SPHERE

M. N'Diaye^a, A. Vigan^{b,c}, K. Dohlen^b, J.-F. Sauvage^{d,b}, A. Caillat^b, A. Costille^b,
J. H. V. Girard^c, J.-L. Beuzit^{e,f}, T. Fusco^{d,b}, P. Blanchard^b, J. Le Merrer^b, D. Le Mignant^b,
F. Madec^b, G. Moreaux^b, D. Mouillet^{e,f}, P. Puget^{e,f}, G. Zins^{c,e,f}

^a Space Telescope Science Institute, 3700 San Martin Drive, Baltimore, MD 21218, USA

^b Aix-Marseille Université, CNRS, LAM UMR 7326, 13388 Marseille, France

^c European Southern Observatory, Alonso de Cordova 3107, Vitacura, Santiago, Chile

^d ONERA, 29 avenue de la Division Leclerc, 92322 Châtillon, France

^e CNRS, IPAG, UMR 5274, B.P. 53, F-38041 Grenoble Cedex 9, France

^f Université Grenoble Alpes, IPAG, 38000 Grenoble, France

ABSTRACT

The high-contrast imaging instruments VLT/SPHERE and GPI have been routinely observing gas giant planets, brown dwarfs, and debris disks around nearby stars since 2013-2014. In these facilities, low-wind effects or differential aberrations between the extreme Adaptive Optics sensing path and the science path represent critical limitations for the observation of exoplanets orbiting their host star with a contrast ratio larger than 10^6 at small separations. To circumvent this problem, we proposed ZELDA, a Zernike wavefront sensor to measure these quasi-static aberrations at a nanometric level. A prototype was installed on VLT/SPHERE during its integration in Chile. We recently performed measurements on an internal source with ZELDA in the presence of Zernike or Fourier modes introduced with the deformable mirror of the instrument. In this communication, we present the results of our experiment and report on the contrast gain obtained with a first ZELDA-based wavefront correction. We finally discuss the suitability of such a solution for a possible upgrade of VLT/SPHERE and for its use with future E-ELT instruments or space missions with high-contrast capabilities (e.g. WFIRST-AFTA, HDST).

Keywords: high angular resolution, coronagraphy, wavefront sensing, wavefront control

1. INTRODUCTION

High-contrast observations with the current facilities on the ground (e.g., VLT/SPHERE,¹ Gemini Planet Imager,² Palomar P1640,³ or Subaru/SCEAO⁴) or in space (e.g. Hubble Space Telescope) enable the direct imaging and spectral analysis of planetary companions or circumstellar disks around nearby stars, thus providing insights on the physical characteristics (mass, orbit) and the chemical composition of disk dust or planet atmosphere. Such information proves extremely valuable to further understand the formation and evolution of planetary systems. Thanks to the combination of extreme adaptive optics (ExAO) to compensate for the atmospheric turbulence effects, coronagraphy to suppress star diffracted light, and observational strategies to efficiently reduce data with post-processing methods, the facilities mounted on large, ground-based observatories can reach contrast ratios between stars and orbiting planets up to $10^5 - 10^6$ at separations smaller than $0.5''$, enabling the observation of warm or massive gaseous planets. However, the presence of speckles in the coronagraphic images impair the observation of colder or lighter planetary companions with a flux ratio larger than 10^6 at separations smaller than $0.3''$.

These speckles originate from the differential aberrations between the ExAO sensing path and the science path of the instrument, the so-called non-common path aberrations (NCPA), which set the limit on the contrast

*E-mail: mamadou@stsci.edu

performance of these exoplanet facilities.⁵ Several strategies were implemented at the time of instrument design to minimize their impact.⁶⁻⁸ In the recently deployed ground-based facilities, NCPA were found to be smaller than expected during the commissioning tests, thanks to the optics quality that was beyond the initial specifications. On VLT/SPHERE, the adopted calibration strategy based on phase diversity⁹ was therefore not found to improve the contrast performance and was thus abandoned.

Still, the remaining NCPA are of the order of a few tens of nanometers, preventing coronagraphs from reaching their ultimate performance (up to 10^7 at $0.2''$). These wavefront errors can be split into two contributions: the long-timescale aberrations that are due to the optical surface errors or misalignments in the instrument optical train and the slowly varying instrumental aberrations that are caused by thermal or opto-mechanical deformations as well as moving optics such as atmospheric dispersion correctors.¹⁰⁻¹² They lead to static to quasi-static speckles in the coronagraphic images that set the contrast threshold of the instrument and prevent the observation of cold or light gaseous exoplanets. Fine and accurate calibration of the errors down to a nanometric level are required to achieve the deepest contrast and expand the discovery space of planetary companions with exoplanet direct imaging instruments.

Over the past few years, several methods have been proposed to measure and correct the residual NCPA.⁶⁻⁸ Of these concepts, the Zernike wavefront sensor represents a compelling solution based on phase-contrast methods because of the simplicity of its optical design for an easy implementation in current instruments and of the ease and accuracy of its reconstruction algorithm for the fast correction of small phase errors at a nanometric level. Over the past fifteen years, such a concept has been investigated in astronomical applications for multiple purposes,¹³ such as wavefront sensing for adaptive optics systems,¹⁴⁻¹⁶ co-phasing for alignment of segmented aperture telescopes,^{17,18} or estimation of low-order aberrations (e.g. pointing errors, focus drifts) for future missions with coronagraphic capabilities.¹⁹⁻²¹ In a previous communication²² we proposed ZELDA, a concept based on the Zernike phase contrast applied to the measurements of quasi-static aberrations in exoplanet direct imaging instruments.²²⁻²⁵

Following our concept studies, we manufactured a prototype that was inserted into VLT/SPHERE in its IR coronagraphic wheel during the re-integration of the instrument at Paranal in 2014. In Dec. 2015, we performed tests that led to the experimental validation of our concept.²⁶ In this communication, we give the main highlights of our demonstration and we show the first results of a ZELDA-based wavefront correction for the calibration of NCPA to reduce the residual speckle brightness in coronagraphic images for exoplanet observation. We then discuss the use of ZELDA in extended applications such as the diagnosis of the unforeseen low-wind effects²⁷ or the estimation of tip, tilt, and piston errors in segmented apertures in the context of exoplanet high-contrast observations with future large segmented aperture telescopes (e.g. E-ELT or LUVOIR such as HDST concept²⁸).

2. ZELDA SENSOR: PRINCIPLE, PROTOTYPE DESIGN, AND PROPERTIES

ZELDA relies on Zernike phase-contrast methods²⁹ to measure NCPA in high-contrast imaging instruments with nanometric accuracy. We briefly recall the principle and formalism of the Zernike sensor.²² We also present the design and prototype for VLT/SPHERE.

ZELDA uses a plane focal phase mask to produce interferences between the reference wave created by the mask and the errors present in the system. The sensor hence converts phase wavefront errors in the entrance pupil plane into intensity variations in the relayed pupil plane, see Fig. 1. The phase-to-intensity conversion depends on the characteristics of the mask, i.e. the diameter d and the introduced phase delay θ . We denote λ and D the wavelength of observation and the telescope aperture diameter.

Assuming small phase errors and a second-order Taylor expansion, the ZELDA signal I_C expresses as a function of φ for a given pixel in the pupil as follows:

$$I_C = P^2 + 2b^2(1 - \cos \theta) + 2Pb [\varphi \sin \theta - (1 - \varphi^2/2)(1 - \cos \theta)] . \quad (1)$$

where P and b denote the amplitude pupil function and the amplitude diffracted by the focal plane phase mask of diameter d .

The phase can be recovered from the intensity by solving this second-order equation. For the design of VLT/SPHERE, we have $d = 1.076\lambda_0/D$ and $\theta = 0.440\pi\lambda_0/\lambda$ with $\lambda_0 = 1.642 \mu\text{m}$. For such a mask size, b has

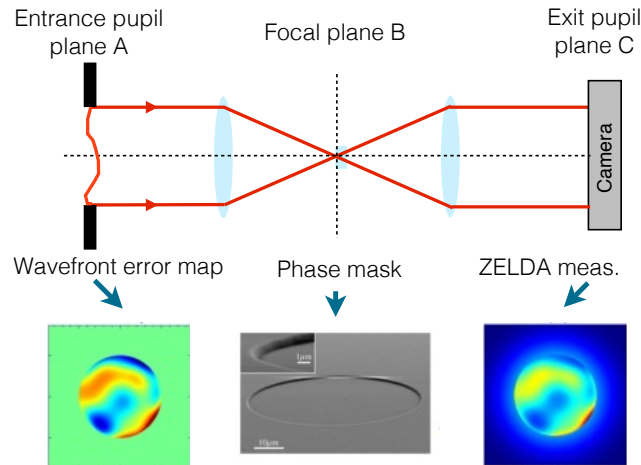


Figure 1. Illustration of the ZELDA concept: wavefront errors at the telescope aperture of diameter D in the entrance pupil plane A forms an aberrated star image in the intermediate focal plane B in which a $\sim \pi/2$ phase-shifting mask of about a resolution element (λ/D) diameter is located. These phase aberrations are converted into intensity variations onto the camera in the relayed pupil plane C. For small aberrations, the phase reconstruction is obtained thanks to a simple and fast algorithm relying on a linear or quadratic relation between the wavefront aberrations and the intensity measurements.

a chromatically dependant profile similar to that of an Airy pattern twice the size of the pupil. Assuming a normalized amplitude in the entrance pupil $P = 1$ and measurements performed at $\lambda = \lambda_0$, the phase error at any point in the pupil is reduced to

$$\varphi = -1.208 + 1.230\sqrt{2.590 - 1.626b - 0.813(1 - I_C)/b}. \quad (2)$$

In H-band, b ranges between 0.4 and 0.65.²⁶ Figure 2 shows the ZELDA signal at $\lambda = \lambda_0$ as a function of the wavefront error for a given pixel with $b = 0.5$. The intensity received by a pixel depends on the wavefront error (WFE) location of that pixel on a sinusoidal function. However, the sinusoid is not symmetric about zero aberration, giving rise to an asymmetric dynamic range defined by the monotonic range around zero. The limits of the dynamic range is given by the changes of gradient sign of I_C , i.e. $dI_C/d\varphi = 0$. In the case of our mask design, the dynamic of the sensor ranges between $-0.14 \lambda_0$ and $0.36 \lambda_0$, as illustrated with the vertical lines in Fig. 2.

For VLT/SPHERE, the phase mask prototype was manufactured by the French company SILIOS technologies. The process consists in machining a cylinder shape into the front face of a fused silica substrate by the aid of masking photolithography and reactive ion etching. Such a method ensures the production of a monolithic phase mask with extremely steep edges and highly precise step depths. Our measurements of the mask with an optical profilometer confirm the excellent shape of the mask made by this procedure, see Figure 3.

3. RESULTS ON VLT/SPHERE

3.1 ZELDA PERFORMANCE

In the end of 2015 we performed multiple validation tests of ZELDA in SPHERE during daytime technical time. This Zernike wavefront sensor was installed in the infrared coronagraphic wheel of the instrument during its reintegration in Paranal in 2014. For our test purposes, the coronagraphic mask is replaced with ZELDA and the system is set up in pupil-imaging mode to perform our phase aberration measurements. Images are taken with the infrared dual-band imager and spectrograph (IRDIS),³⁰ one of the two scientific subsystems of SPHERE for the near-infrared detection and characterization of giant planets.^{31,32}

During these tests, we introduced Zernike and Fourier modes on the SPHERE high-order deformable mirror (DM) to cover low-order aberrations and spatial frequencies, which are the main components of the NCPA that

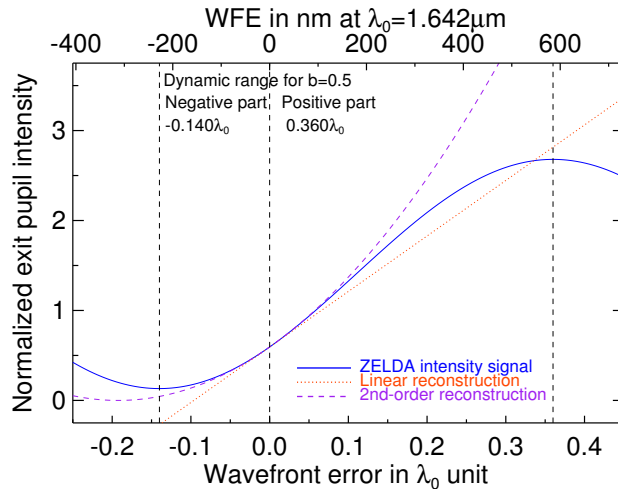


Figure 2. ZELDA pupil plane intensity as a function of the entrance pupil plane wavefront error (blue curve) for a mask with 0.440π phase delay and $1.076 \lambda_0/D$ diameter in H-band ($\lambda_0=1.642 \mu\text{m}$). The plot is displayed for a mask amplitude diffracted wave that is equal to half the entrance pupil amplitude ($b=0.5$). Note the asymmetry of the sensor dynamic with values ranging from -0.14 to $0.36 \lambda_0$. The linear and quadratic phase reconstruction are represented with the red dotted-line and purple dashed-line curves.

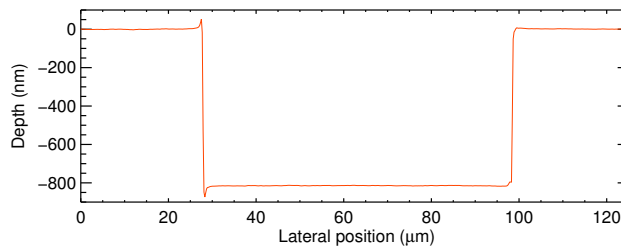


Figure 3. General profile of the phase mask measured by profilometry using a Wyko interference microscope. The mask presents measured depth and diameter $70.7 \mu\text{m}$ and 814.6 nm , which are consistent to within 1% and 0.1% with the specifications and accuracy range of the process.

we want to correct to improve the performance of an ExAO coronagraphic system. We compared the ZELDA measurements with the theoretical modes at various amplitudes to estimate the performance and explore the dynamic range of the sensor. In this section we briefly describe the data acquisition and analysis before reviewing the results obtained with different modes.

3.1.1 Calibration of the introduced aberrations

For optimal performance, the modes were introduced in the system in closed-loop mode using an offset to the reference slopes of the Shack-Hartmann (SH) wavefront sensor (WFS) of SPHERE. This approach allowed us to benefit from an extremely high-quality point-spread function (PSF, Strehl ratio $> 90\%$ at λ_0) at the level of the ZELDA phase mask, since the system works fully in closed-loop mode.

We also calibrate the amount of the requested aberrations that are introduced with the DM. Using a ramp of introduced defocus, we estimate the Strehl ratio at the level of the PSF and fit it with Marechal's approximation to estimate the defocus and compare it with the introduced mode in order to determine a sensitivity factor. To project the aberration phase map onto the reference slopes, the calibrated interaction matrix of the AO loop is used. This matrix represents the sensitivity of the SH-WFS to all the modes controlled by the system, it therefore accounts for the system response as accurately as possible. The sensitivity factor is hence valid for any other mode, although it has been calibrated only on the focus.

3.1.2 Data acquisition, processing, and analysis

All measurements were made internally using the light sources available in the calibration unit of the instrument.³³ Images are taken with IRDIS and an exposure time of 10 seconds is used, providing a signal-to-noise ratio high enough for the analysis. The whole set of acquired data can be found in Ref.²⁶ At the beginning of each data acquisition session, we performed the calibration of the sensitivity factor to ensure an accurate knowledge of the amount of aberrations introduced in the ZELDA tests.

We performed the main tests with Zernike and Fourier modes to analyze the performance of ZELDA over several spatial frequencies. For each test, the PSF was manually centered on the ZELDA phase mask by looking at the pupil intensity image on the IRDIS detector. Since ZELDA transforms phase errors into intensity variations, performing an accurate centering visually is relatively easy, especially since the overall amount of aberrations in SPHERE is low.³⁴ The PSF is centered by changing the reference slopes of the near-IR differential tip-tilt sensor (DTTS) of the instrument, the purpose of which is to maintain the PSF centered and stable on the coronagraph. As a result, the tip-tilt cannot be controlled directly with the reference slopes of the SH-WFS because the DTTS will ensure that the PSF is always centered on the same location. For the tip-tilt tests with ZELDA, the DTTS loop was opened to disable this control of the centering and allow the PSF to move freely.

For each test, three types of data were acquired: ZELDA data with the PSF centered on the phase mask, a clear pupil reference with the PSF outside of the phase mask to obtain the contribution of the amplitude aberrations, and instrumental backgrounds. All data were acquired with ramps of aberrations in the Fe II near-IR narrow-band filter centered on $\lambda = 1642$ nm ($\Delta\lambda = 24$ nm), for which the ZELDA phase mask was originally designed.

The Zernike modes were calculated on an annular geometry³⁵ to take into account the central actuators of the SPHERE DM that are not seen by the SH-WFS and are not controlled in closed-loop mode by the system. The Fourier modes were tested up to ten cycles/pupil in both horizontal and vertical directions (x and y). After acquisition, the data of each sequence were processed uniformly. The images were first background subtracted, and the bad pixels were corrected for using a sigma-clipping procedure. Then we normalized the ZELDA pupil image by the clear pupil image itself for each pixel, and finally, for each aberration and amplitude, we calculated the phase from the normalized ZELDA images following Eq. (2).

Figure 4 shows all the annular Zernike modes measured with ZELDA in the system when we introduced 400 nm PtV of aberrations. The central actuators, not seen by the WFS and controlled by the system, have been numerically masked out. Overall, the shape of the Zernike modes is well reproduced and clearly recognizable. The regular pattern of the DM actuators is clearly visible, as is the effect of individual dead or stuck and known actuators.

3.1.3 Results for different modes

In our tests on SPHERE, the introduced aberration was measured by ZELDA for different error sources: the quasi-static aberrations in our system, dead actuators in the DM, the photon noise and detector readout noise. For each mode, we adopted a differential data analysis strategy with measurements with and without introduced aberration to minimize the effect of quasi-static errors on the ZELDA measurement. The photon and detector noises are small thanks to the high signal-to-noise (S/N) ratio of the original images. The dead actuators on the DM generate large amplitude errors that go beyond the dynamic range of ZELDA, making the aberrations at the corresponding pupil locations challenging to estimate. We ruled out the dead actuator points in our measurement map with a numerical mask. From the resulting measurement points, we fit the measured aberration with a function representing the introduced aberration to mitigate the remaining error sources (residual errors, the photon noise and detector noise) and derived the aberration amplitude that was experimentally measured by our Zernike sensor.

For comparison to the experimental result, we numerically modeled the theoretical ZELDA measurement for the introduced amplitude on DM in the absence of noise. As for experimental data, we excluded the points that are measured at the location of dead actuators.

Figure 5 displays the theoretical and experimental measurements of the Zernike sensor for tip-tilt and defocus, showing good agreement between theory and experience. The same general behavior has been observed with

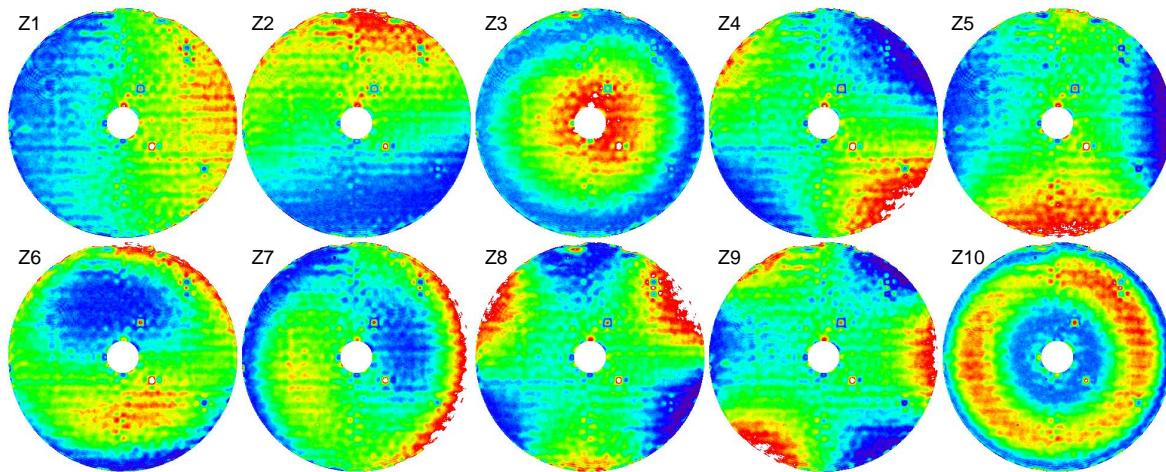


Figure 4. Illustration of the ZELDA measurements on VLT/SPHERE for the first 10 different Zernike modes introduced on the DM with 400 nm peak-to-valley amplitude. The shape of these modes can easily be recognized from these maps. In addition, the regular actuator pattern is clearly visible from these maps. The dead or stuck actuators are visible in black or white as their corresponding phase are found out far beyond the ZELDA dynamic range. The actuators visible at the edge of the pupil central obscuration (14% of the pupil in diameter, numerically masked in these maps) are not dead or stuck, but they are not controlled properly because they significantly overlap with the central obscuration.

other Zernike modes and Fourier modes, as reported in Ref.²⁶ The discrepancies between theory and experiment are thought to be related to the accurate calibration of the sensitivity factor. We note that the value of the sensitivity factor varies by up to 10% from one day to the next. No systematic measurements were made to quantify the variations at higher temporal frequency, but it is reasonable to assume that some variations can be expected over the course of 5-6 hours (typical length of our data acquisition sessions), leading to the small differences observed with respect to the theory.

The Zernike sensor shows a linear response around the zero point, enabling a simple reconstruction of the small coronagraphic aberrations and fast convergence with close-loop compensation toward the zero point in one or two iterations. In this regime, the slope of the response curve is equal to one for all the Zernike modes except for the tip-tilt errors. This behavior is believed to be due to the modification of the light distribution going through the decentered mask with respect to the star image.²² With a careful calibration, this effect will have no impact on the ability of the Zernike sensor to measure tip-tilt errors.

For the aberrations outside the linear range, the Zernike sensor still proves efficient by considering a close-loop operation between with the measurement and correction. The measurements converge towards the linear regime of the wavefront sensor after a few iterations.¹⁸ Since ZELDA is assumed to operate in the presence of small aberrations, our data analysis is based on a quadratic relation between the measured intensity and the wavefront errors. More accurate reconstruction expression will further be investigated to increase the accuracy for large phase errors.

We also performed tests using different filters to probe the sensitivity of ZELDA to spectral bandpass.²⁶ By knowing the filter characteristics (central wavelength, bandwidth) and taking them into account in the data analysis, ZELDA performs accurate aberration measurement using filters with a wide spectral band ($\Delta\lambda=290$ nm) or centered on a wavelength largely shifted from the wavelength of design ($\lambda_c = 2124$ nm instead of $\lambda_0 = 1642$ nm, i.e., a shift of 482 nm).

3.2 RESULTS WITH ZELDA-BASED WAVEFRONT CORRECTION

We now use ZELDA to measure and compensate for the NCPA of SPHERE at the level of the coronagraphic mask to improve the quality of the focal-plane images. First, the amount of aberrations introduced when changing the reference slopes was calibrated. Then a ZELDA measurement was acquired and analyzed to produce an optical path difference (OPD) map, which is presented in the top left of Fig. 6. In addition to the static pattern of DM

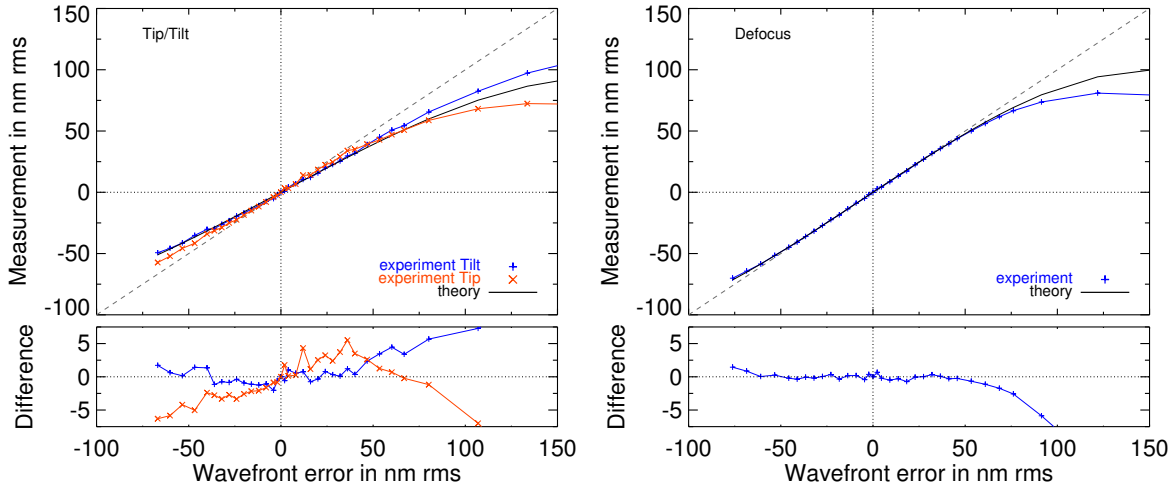


Figure 5. **Top:** ZELDA measurements as a function of the wavefront errors for tip-tilt (left plot) and defocus (right) modes in theory (black curve) and during our experiment on VLT/SPHERE (colored curves). **Bottom:** Difference between the experimental and theoretical measurements. Our experimental results are very consistent with numerical simulations for the theory. The observed small discrepancies are believed to be due to source errors: the quasi-static aberrations in our system, dead actuators in the DM, the photon noise and detector readout noise.

actuators, the OPD map clearly shows low spatial frequency aberrations at the level of a few dozen nanometers (RMS), corresponding to uncorrected NCPA.

3.2.1 ZELDA maps before and after NCPA correction

This map cannot be projected directly onto the reference slopes of the SH-WFS since with the pupil sampling on IRDIS detector, ZELDA is sensitive to spatial frequencies up to 190 cycles/pupil while SPHERE high-order DM can only control frequencies up to 20 cycles/pup. To avoid any spatial aliasing, the ZELDA OPD map was first filtered in Fourier space using a Hann window of size $25 \lambda/D$ (Fig. 6, bottom row) to avoid filtering or attenuation of the spatial frequencies that could be corrected with the DM. Due to our limited time with the instrument, we did not investigate other filters but we plan to probe other filtering windows in further tests.

The filtered OPD map was then projected onto the reference slopes of the WFS, and a new ZELDA image was acquired and analysed, providing the OPD map showed in Fig. 6, top right panel. In this new OPD map, the low spatial frequencies have now completely disappeared, and the map appears much flatter, showing an apparent correction of the NCPA of the system.

A slight residual tip-tilt in the OPD map after correction remains, particularly visible in the Hann-filtered version of the OPD map. This is not the result of an imperfect measurement, but simply arises because the tip-tilt is controlled in close-loop mode by the DTTS, for which the reference slopes are changed manually at the beginning of the test to center the PSF on the ZELDA mask. The optimal approach would be to correct the high orders by modifying the reference slopes of the SH WFS and to correct the tip-tilt by modifying the reference slopes of the DTTS. We were unable to investigate this approach for the tests presented here, but it will represent a necessary improvement in future tests.

3.2.2 Coronagraphic images before and after NCPA correction

To check the quality of the NCPA compensation, we acquired coronagraphic images with IRDIS at 1593 nm (H2 filter³²), using the Apodized Pupil Lyot Coronagraph (APLC)³⁶ optimized for the *H* band. Two data sets were acquired: one using the default reference slopes of the WFS (before correction), and one using the reference slopes updated using the ZELDA measurement (after correction). For each data set, we acquired a 2 min coronagraphic image and 2 min reference PSF image where the PSF was moved out of the coronagraphic mask. A neutral density filter was used to acquire the reference PSF without saturating the peak. Corresponding instrumental backgrounds were also acquired.

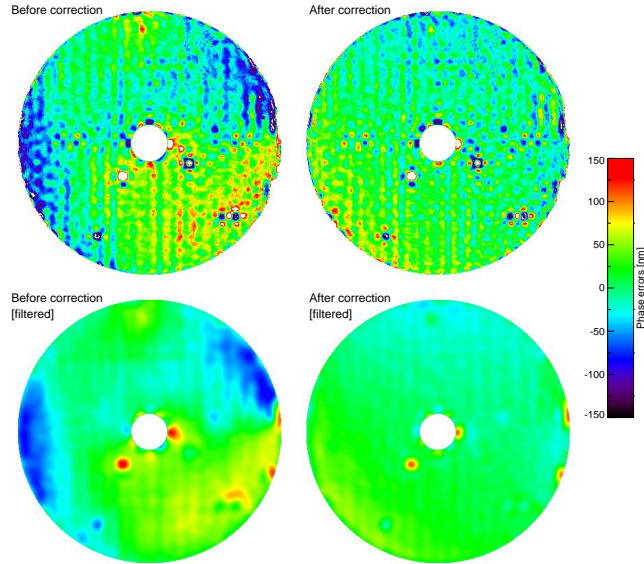


Figure 6. **Top:** Illustration of the ZELDA measured phase maps of the noncommon path aberrations (NCPA) on VLT/SPHERE using IRDIS before and after correction of these errors. **Bottom:** Same maps but filtered in Fourier map with a Hann window of size $25 \lambda/D$ to avoid any spatial aliasing. Low spatial frequency aberrations are clearly visible on the left, while they have disappeared after the correction, except for a small amount of residual tip-tilt.

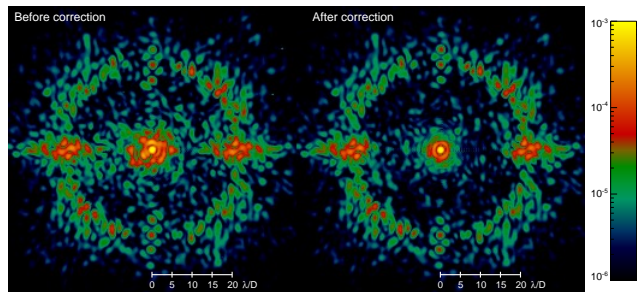


Figure 7. Coronagraphic images measured at 1593 nm (IRDIS H2 filter) before and after the compensation of non common path aberrations thanks to the ZELDA measurements showed in Fig. 6. Images are showed on the color scale. A contrast gain is clearly visible close to the star image center but also farther out where the intensity of the speckles in the deformable mirror controlled area has decreased significantly.

The resulting coronagraphic images are showed in Fig. 7. The visual difference between the two images is striking inside the AO-corrected area. After the NCPA correction, the whole AO-corrected region appears much cleaner: the speckles close to the axis have almost disappeared to reveal a very regular annulus at the edge of the coronagraphic mask, similar to what is expected from the theoretical APLC design of SPHERE.³⁷ In the $4-8 \lambda/D$ range, the static speckles are also strongly attenuated. In the remaining AO-corrected region, the speckles are also attenuated, which is particularly visible along the horizontal and vertical directions, where a strong static pattern of speckles was previously visible.

To quantitatively assess the performance gain after NCPA compensation, we plot in Fig. 8 the azimuthal standard deviation profile of the coronagraphic images as a function of separation, normalized to the peak flux of the reference off-axis PSF. The bottom panel of the figure shows the gain in contrast between the two curves. Within $2-16 \lambda/D$, there is a gain in contrast of a factor more than 2, with even a peak at more than 10 around $5 \lambda/D$. This agrees very well with our previous estimates,²² where we estimated a possible gain over a factor of 10, and it is a strong confirmation of the potential of ZELDA to compensate for NCPA.

We also plot the simulated theoretical performance of the SPHERE APLC in presence of the amplitude aberrations directly measured in the instrument and using an image of the Lyot stop, but without any phase

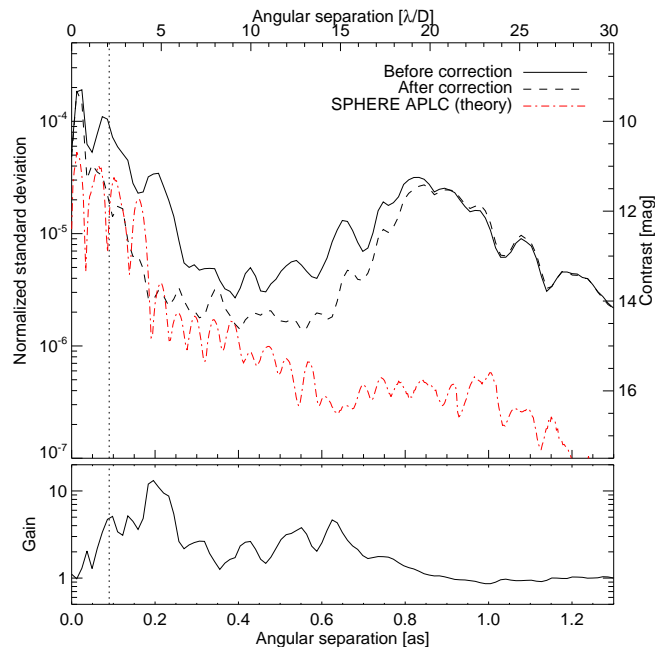


Figure 8. Normalized azimuthal standard deviation profiles before (plain line) and after (dashed line) correction of the NCPA using ZELDA, as a function of angular separation. The contrast gain is plotted in the bottom panel. The dotted line corresponds to the edge of the coronagraphic mask (90 mas). The measurements correspond to the coronagraphic images presented in Fig. 7. They are compared to the theoretical performance of the SPHERE APLC (red, dash-dotted line).

aberrations. Within $5 \lambda/D$, we reach this theoretical performance, which means that the NCPA at low spatial frequencies are almost entirely corrected for. We note that on the internal source the instrument pupil is purely circular, with no central obscuration or spiders, but the Lyot stop still includes elements to mask the diffraction of the central obscuration, the spiders, and the bad actuators of the DM. This will result in a slightly better performance of the coronagraph on sky than on the internal source.

4. LOW-WIND EFFECTS

Unforeseen limiting effects have been experienced with the recently deployed high-contrast imaging instruments of unprecedented performance.²⁷ Of these limitations, the low-wind effects (LWE) appear when the outdoor wind speed (i.e., 30 m below the VLT platform) is below 1 to 3 m/s.²⁷ In the monolithic telescope pupil, this generates piston pattern across the spiders with phase steps up to hundreds of nanometers, leading to a clear degradation of the star image quality with the presence of strong speckles in the PSF first bring diffraction ring and even a splitting of the main PSF peak into four peaks of varying intensity, see Fig. 9. Such effects strongly impact the science operations with a loss of about 20% of the observing time.

The cause of this effect has recently been identified as being energetic transfer between spiders that are radiatively cooled by the night sky, and the slowly passing dome air. While strategies such as repainting spiders using a low-emissivity paint are being studied to control the root cause of this particular case of dome seeing, real-time phase measurements may be needed to correct for its effect.

In October 2014, the ZELDA sensor was used on SPHERE during the commissioning operations to observe and understand this effect. Figure 10 shows an example of ZELDA intensity measurement on sky during a moderate case of LWE. The phase map clearly shows discontinuities at the level of the spiders struts. A zoomed phase map on the right image is displayed with an area which size that is equal to $1/40$ of the pupil diameter, corresponding to the subaperture of the SH-WFS. Such an image underlines the sharpness of the discontinuity and the difficulty for the measurement and modeling of this effect with the with a 30% coupling influence function of the high-order DM.²⁷

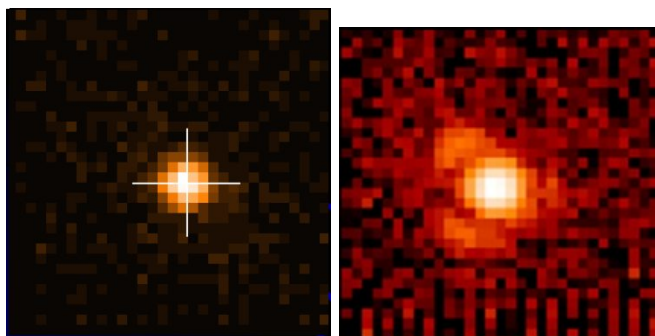


Figure 9. On-sky images of an observed star with the VLT/SPHERE in the absence or not of low-wind effects (LWE). The image quality is clearly altered with this limitation, reducing the ability of exoplanet direct imaging instruments to produce high-contrast observations of circumstellar environments, strongly impacting the time for science operations.

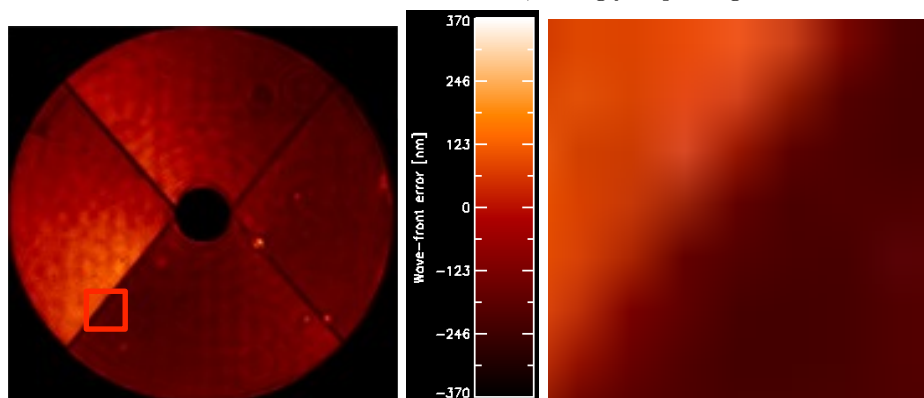


Figure 10. On-sky measurements of ZELDA in the presence of low-wind effects. The left image show evidence of piston effects between the four quadrants of the telescope. The right image shows a subset of the previous measurement at the spider strut discontinuity (red box) over a SH WFS sub-aperture which size is equal to $1/40$ of the pupil diameter. The transition is narrower than the size of an sub-aperture. The aberration presents dstrong discontinuities with phase step up to hundreds of nanometers peak-t-o-valley wavefront error.

Thanks to its capture range (Fig. 2), our Zernike sensor is able to measure LWE with amplitudes up to 800 nm in the near infrared. We also model images from ZELDA measurements to compare them with the images obtained at the DTTS in SPHERE. Both sets of images have showed good consistency, enabling the validation of ZELDA as a good wavefront sensor for the LWE measurement.²⁷

5. CONCLUSION AND PERSPECTIVES

We have validated ZELDA, a sensor based on Zernike phase contrast methods to measure the NCPA present on exoplanet direct-imaging instruments with nanometric accuracy. With our installed prototype on SPHERE and using internal source, we have performed experimental tests and showed the ability of our sensor to measure Zernike or Fourier modes that are the main contributors of the NCPA. We have thus calibrated the NCPA on SPHERE based on the ZELDA measurements, resulting in an improvement of the coronagraphic image quality and a contrast gain up to 10 in the search area in which the gas giant planets are expected to be observed. ZELDA has also proven to be an excellent and efficient tool to diagnose the low-wind effects, a devastating effect in high-contrast facilities that was unforeseen at the time of the instrument design. Our results are very encouraging in the perspective of having ZELDA as a possible upgrade of SPHERE to measure NCPA and reach the ultimate contrast limits of the instrument.

From a practical point of view, the NCPA correction with ZELDA in SPHERE could be implemented following two approaches. The *off-line* approach, in which the NCPA would be measured at the beginning of the night, and the same correction would be applied to all observations during that night. This assumes that most of the NCPA do not vary significantly over the course of a few hours. This is similar to the original calibration scheme foreseen for the instrument, where the NCPA would be calibrated once per day using phase diversity techniques.⁹ The *online* approach is more complex to implement since it requires replacing the entire near-infrared DTTS with a ZELDA-based sensor. The main gain of the *online* implementation is that it allows sensing not only tip-tilt variations but also higher-order NCPA in real-time during the observations, providing the equivalent of the calibration wavefront sensor in the Gemini/GPI instrument.⁷ This solution is currently under study for future evolutions of SPHERE.

Additional ZELDA applications are also currently under investigation. For instance, since ZELDA provides a high-resolution phase map of the pupil, this sensor can be extremely useful for fine segment cophasing thanks to the direct measurement of piston, tip and tilt of individual segments it provides. ZELDA is a well suited sensor for the measurement of residual cophasing errors on ELTs. Current high-contrast imaging facilities and future exoplanet direct imagers on ELTs or envisioned post-JWST space observatories²⁸ might thus benefit from the ZELDA-based wavefront correction to increase the signal-to-noise ratio of the planetary companions in the coronagraphic images and hence expand the discovery space of observable exoplanets by reaching deeper contrasts at small angular separations. Such a solution is currently considered for E-ELT/HARMONI and its high-contrast imaging mode for exoplanet studies.

ACKNOWLEDGMENTS

This work is partially supported by the National Aeronautics and Space Administration under grants NNX12AG05G and NNX14AD33G issued through the Astrophysics Research and Analysis (APRA) program (PI: R. Soummer). MN would like to thank R. Soummer and L. Pueyo for their support. MN would also like to acknowledge the ESO Chile Visiting Scientist program. Finally, AV would like to thank the Paranal staff for their patience and support when performing the tests presented in this work.

SPHERE is an instrument designed and built by a consortium consisting of IPAG (Grenoble, France), MPIA (Heidelberg, Germany), LAM (Marseille, France), LESIA (Paris, France), Laboratoire Lagrange (Nice, France), INAF - Osservatorio di Padova (Italy), Observatoire de Genève (Switzerland), ETH Zurich (Switzerland), NOVA (Netherlands), ONERA (France) and ASTRON (Netherlands) in collaboration with ESO. SPHERE was funded by ESO, with additional contributions from CNRS (France), MPIA (Germany), INAF (Italy), FINES (Switzerland) and NOVA (Netherlands). SPHERE also received funding from the European Commission Sixth and Seventh Framework Programmes as part of the Optical Infrared Coordination Network for Astronomy (OPTICON) under grant number RII3-Ct-2004-001566 for FP6 (2004-2008), grant number 226604 for FP7 (2009-2012) and grant number 312430 for FP7 (2013-2016).

REFERENCES

- [1] Beuzit, J., Feldt, M., Dohlen, K., Mouillet, D., Puget, P., Wildi, F., Abe, L., Antichi, J., Baruffolo, A., Baudoz, P., Boccaletti, A., Carbillet, M., Charton, J., Claudi, R., Downing, M., Fabron, C., Feautrier, P., Fedrigo, E., Fusco, T., Gach, J., Gratton, R., Henning, T., Hubin, N., Joos, F., Kasper, M., Langlois, M., Lenzen, R., Moutou, C., Pavlov, A., Petit, C., Pragt, J., Rabou, P., Rigal, F., Roelfsema, R., Rousset, G., Saisse, M., Schmid, H., Stadler, E., Thalmann, C., Turatto, M., Udry, S., Vakili, F., and Waters, R., "SPHERE: a planet finder instrument for the VLT," in [*SPIE*], **7014** (Aug. 2008).
- [2] Macintosh, B., Graham, J. R., Ingraham, P., Konopacky, Q., Marois, C., Perrin, M., Poyneer, L., Bauman, B., Barman, T., Burrows, A. S., Cardwell, A., Chilcote, J., De Rosa, R. J., Dillon, D., Doyon, R., Dunn, J., Erikson, D., Fitzgerald, M. P., Gavel, D., Goodsell, S., Hartung, M., Hibon, P., Kalas, P., Larkin, J., Maire, J., Marchis, F., Marley, M. S., McBride, J., Millar-Blanchaer, M., Morzinski, K., Norton, A., Oppenheimer, B. R., Palmer, D., Patience, J., Pueyo, L., Rantakyro, F., Sadakuni, N., Saddlemyer, L., Savransky, D., Serio, A., Soummer, R., Sivaramakrishnan, A., Song, I., Thomas, S., Wallace, J. K., Wiktorowicz, S., and Wolff, S., "First light of the Gemini Planet Imager," *Proceedings of the National Academy of Science* **111**, 12661–12666 (Sept. 2014).

- [3] Hinkley, S., Oppenheimer, B. R., Zimmerman, N., Brenner, D., Parry, I. R., Crepp, J. R., Vasisht, G., Ligon, E., King, D., Soummer, R., Sivaramakrishnan, A., Beichman, C., Shao, M., Roberts, L. C., Bouchez, A., Dekany, R., Pueyo, L., Roberts, J. E., Lockhart, T., Zhai, C., Shelton, C., and Burruss, R., “A New High Contrast Imaging Program at Palomar Observatory,” *Public. of the Astron. Soc. Pac.* **123**, 74–86 (Jan. 2011).
- [4] Guyon, O., Martinache, F., Garrel, V., Vogt, F., Yokochi, K., and Yoshikawa, T., “The Subaru coronagraphic extreme AO (SCEXAO) system: wavefront control and detection of exoplanets with coherent light modulation in the focal plane,” in [*Society of Photo-Optical Instrumentation Engineers (SPIE) Conference Series*], **7736** (July 2010).
- [5] Fusco, T., Rousset, G., Sauvage, J.-F., Petit, C., Beuzit, J.-L., Dohlen, K., Mouillet, D., Charton, J., Nicolle, M., Kasper, M., Baudoz, P., and Puget, P., “High-order adaptive optics requirements for direct detection of extrasolar planets: Application to the SPHERE instrument,” *Optics Express* **14**, 7515 (2006).
- [6] Gonsalves, R. A., “Phase retrieval and diversity in adaptive optics,” *Optical Engineering* **21**, 829–832 (Oct. 1982).
- [7] Wallace, J. K., Burruss, R. S., Bartos, R. D., Trinh, T. Q., Pueyo, L. A., Fregoso, S. F., Angione, J. R., and Shelton, J. C., “The Gemini Planet Imager calibration wavefront sensor instrument,” in [*Society of Photo-Optical Instrumentation Engineers (SPIE) Conference Series*], **7736** (July 2010).
- [8] Paul, B., Sauvage, J.-F., and Mugnier, L. M., “Coronagraphic phase diversity: performance study and laboratory demonstration,” *Astron. & Astrophys.* **552**, A48 (Apr. 2013).
- [9] Sauvage, J.-F., Fusco, T., Rousset, G., and Petit, C., “Calibration and precompensation of noncommon path aberrations for extreme adaptive optics,” *Journal of the Optical Society of America A* **24**, 2334–2346 (Aug. 2007).
- [10] Macintosh, B., Poyneer, L., Sivaramakrishnan, A., and Marois, C., “Speckle lifetimes in high-contrast adaptive optics,” in [*Astronomical Adaptive Optics Systems and Applications II. Edited by Tyson, Robert K.; Lloyd-Hart, Michael. Proceedings of the SPIE, Volume 5903, pp. 170-177 (2005).*], Tyson, R. K. and Lloyd-Hart, M., eds., **5903**, 170–177 (Aug. 2005).
- [11] Martinez, P., Loose, C., Aller Carpentier, E., and Kasper, M., “Speckle temporal stability in XAO coronagraphic images,” *Astron. & Astrophys.* **541**, A136 (May 2012).
- [12] Martinez, P., Kasper, M., Costille, A., Sauvage, J. F., Dohlen, K., Puget, P., and Beuzit, J. L., “Speckle temporal stability in XAO coronagraphic images. II. Refine model for quasi-static speckle temporal evolution for VLT/SPHERE,” *Astron. & Astrophys.* **554**, A41 (June 2013).
- [13] Dohlen, K., “Phase masks in astronomy: From the Mach-Zehnder interferometer to coronagraphs,” in [*EAS Publications Series*], Aime, C. and Soummer, R., eds., **12**, 33–44 (2004).
- [14] Bloemhof, E. E. and Wallace, J. K., “Phase contrast techniques for wavefront sensing and calibration in adaptive optics,” in [*SPIE*], **5169**, 309–320 (Dec. 2003).
- [15] Bloemhof, E. E. and Wallace, J. K., “Phase-contrast wavefront sensing for adaptive optics,” in [*SPIE*], Gonglewski, J. D., Gruneisen, M. T., and Giles, M. K., eds., **5553**, 159–169 (Oct. 2004).
- [16] Wallace, J. K., Rao, S., Jensen-Clem, R. M., and Serabyn, G., “Phase-shifting Zernike interferometer wavefront sensor,” in [*Society of Photo-Optical Instrumentation Engineers (SPIE) Conference Series*], **8126** (Sept. 2011).
- [17] Surdej, I., Yaitskova, N., and Gonté, F., “On-sky performance of the Zernike phase contrast sensor for the phasing of segmented telescopes,” *Applied Optics* **49**, 4052 (July 2010).
- [18] Vigan, A., Dohlen, K., and Mazzanti, S., “On-sky multiwavelength phasing of segmented telescopes with the Zernike phase contrast sensor,” *Applied Optics* **50**, 2708 (June 2011).
- [19] Spergel, D., Gehrels, N., Breckinridge, J., Donahue, M., Dressler, A., Gaudi, B. S., Greene, T., Guyon, O., Hirata, C., Kalirai, J., Kasdin, N. J., Moos, W., Perlmutter, S., Postman, M., Rauscher, B., Rhodes, J., Wang, Y., Weinberg, D., Centrella, J., Traub, W., Baltay, C., Colbert, J., Bennett, D., Kiessling, A., Macintosh, B., Merten, J., Mortonson, M., Penny, M., Roza, E., Savransky, D., Stapelfeldt, K., Zu, Y., Baker, C., Cheng, E., Content, D., Dooley, J., Foote, M., Goullioud, R., Grady, K., Jackson, C., Kruk, J., Levine, M., Melton, M., Peddie, C., Ruffa, J., and Shaklan, S., “WFIRST-2.4: What Every Astronomer Should Know,” *ArXiv e-prints* (May 2013).

- [20] Spergel, D., Gehrels, N., Baltay, C., Bennett, D., Breckinridge, J., Donahue, M., Dressler, A., Gaudi, B. S., Greene, T., Guyon, O., Hirata, C., Kalirai, J., Kasdin, N. J., Macintosh, B., Moos, W., Perlmutter, S., Postman, M., Rauscher, B., Rhodes, J., Wang, Y., Weinberg, D., Benford, D., Hudson, M., Jeong, W.-S., Mellier, Y., Traub, W., Yamada, T., Capak, P., Colbert, J., Masters, D., Penny, M., Savransky, D., Stern, D., Zimmerman, N., Barry, R., Bartusek, L., Carpenter, K., Cheng, E., Content, D., Dekens, F., Demers, R., Grady, K., Jackson, C., Kuan, G., Kruk, J., Melton, M., Nemati, B., Parvin, B., Poberezhskiy, I., Peddie, C., Ruffa, J., Wallace, J. K., Whipple, A., Wollack, E., and Zhao, F., “Wide-Field Infrared Survey Telescope-Astrophysics Focused Telescope Assets WFIRST-AFTA 2015 Report,” *ArXiv e-prints* (Mar. 2015).
- [21] Zhao, F., “WFIRST-AFTA coronagraph instrument overview,” in [*SPIE*], **9143**, 0 (Aug. 2014).
- [22] N’Diaye, M., Dohlen, K., Fusco, T., and Paul, B., “Calibration of quasi-static aberrations in exoplanet direct-imaging instruments with a Zernike phase-mask sensor,” *Astron. & Astrophys.* **555**, A94 (July 2013).
- [23] N’Diaye, M., Dohlen, K., Fusco, T., El Hadi, K., Soummer, R., Cuevas, S., Zerrad, M., and Ferrari, M., “Lab results of the circular phase mask concepts for high-contrast imaging of exoplanets,” in [*SPIE*], **8450** (Sept. 2012).
- [24] Dohlen, K., Madec, F., N’Diaye, M., Paul, B., Fusco, T., Jolivet, A., Luo, D., Yatcheva, L., Sauvage, J.-F., Mugnier, L., and Ferrari, M., “Lab demonstration of the Zernike phase mask near-coronagraph quasi static aberrations sensor, ZELDA,” in [*Proceedings of the Third AO4ELT Conference*], Esposito, S. and Fini, L., eds., 86 (Dec. 2013).
- [25] N’Diaye, M., Dohlen, K., Caillat, A., Costille, A., Fusco, T., Jolivet, A., Madec, F., Mugnier, L., Paul, B., Sauvage, J.-F., Soummer, R., Vigan, A., and Wallace, J. K., “Design optimization and lab demonstration of ZELDA: a Zernike sensor for near-coronagraph quasi-static measurements,” in [*SPIE*], **9148**, 5 (Aug. 2014).
- [26] N’Diaye, M., Vigan, A., Dohlen, K., Sauvage, J.-F., Caillat, A., Costille, A., Girard, J. H. V., Beuzit, J.-L., Fusco, T., Blanchard, P., Le Merrer, J., Le Mignant, D., Madec, F., Moreaux, G., Mouillet, D., Puget, P., and Zins, G., “Calibration of quasi-static aberrations in exoplanet direct-imaging instruments with a Zernike phase-mask sensor. II. Concept validation with ZELDA on VLT/SPHERE,” *Astron. & Astrophys. accepted* (June 2016).
- [27] Sauvage, J. F., Fusco, T., Andres, G., Wizinowich, P., O’Neal, J., N’Diaye, M., Vigan, A., Girard, J., Lesur, G., Mouillet, D., Beuzit, J.-L., Kasper, M., Le Louarn, M., Milli, J., Dohlen, K., Neichel, B., Bourget, P., Hagenauer, P., and Mawet, D., “Low Wind Effect, the main limitation of the SPHERE instrument,” in [*Proceedings of the Fourth AO4ELT Conference*], Esposito, S. and Fini, L., eds. (2016).
- [28] Dalcanton, J., Seager, S., Aigrain, S., Battel, S., Brandt, N., Conroy, C., Feinberg, L., Gezari, S., Guyon, O., Harris, W., Hirata, C., Mather, J., Postman, M., Redding, D., Schiminovich, D., Stahl, H. P., and Tumlinson, J., “From Cosmic Birth to Living Earths: The Future of UVOIR Space Astronomy,” *ArXiv e-prints* (July 2015).
- [29] Zernike, F., “Diffraction theory of the knife-edge test and its improved form, the phase-contrast method,” *Mon. Not. of the Royal Astron. Soc.* **94**, 377–384 (Mar. 1934).
- [30] Dohlen, K., Langlois, M., Saisse, M., Hill, L., Origne, A., Jacquet, M., Fabron, C., Blanc, J.-C., Llored, M., Carle, M., Moutou, C., Vigan, A., Boccaletti, A., Carbillet, M., Mouillet, D., and Beuzit, J.-L., “The infrared dual imaging and spectrograph for SPHERE: design and performance,” in [*SPIE Conference Series*], **7014**, 3 (July 2008).
- [31] Vigan, A., Langlois, M., Moutou, C., and Dohlen, K., “Exoplanet characterization with long slit spectroscopy,” *Astron. & Astrophys.* **489**, 1345–1354 (Oct. 2008).
- [32] Vigan, A., Moutou, C., Langlois, M., Allard, F., Boccaletti, A., Carbillet, M., Mouillet, D., and Smith, I., “Photometric characterization of exoplanets using angular and spectral differential imaging,” *Mon. Not. of the Royal Astron. Soc.* **407**, 71–82 (Sept. 2010).
- [33] Wildi, F., Mouillet, D., Beuzit, J.-L., Feldt, M., Dohlen, K., Fusco, T., Petit, C., Desidera, S., Gratton, R., Schmid, H.-M., Langlois, M., Vigan, A., Charton, J., Claudi, R., Roelfsema, R., Baruffolo, A., and Puget, P., “Calibrating SPHERE, the exo-planet imager for the VLT,” in [*SPIE Conference Series*], **7440**, 0 (Aug. 2009).

- [34] Vigan, A., N'Diaye, M., Dohlen, K., Beuzit, J.-L., Costille, A., Caillat, A., Baruffolo, A., Blanchard, P., Carle, M., Ferrari, M., Fusco, T., Gluck, L., Hugot, E., Jaquet, M., Langlois, M., Le Mignant, D., Llored, M., Madec, F., Mouillet, D., Origné, A., Puget, P., Salasnich, B., and Sauvage, J.-F., “Apodization in high-contrast long-slit spectroscopy. II. Concept validation and first on-sky results with VLT/SPHERE,” *Astron. & Astrophys.* **586**, A144 (Feb. 2016).
- [35] Mahajan, V. N., “Zernike annular polynomials for imaging systems with annular pupils,” *Journal of the Optical Society of America (1917-1983)* **71**, 75–85 (1981).
- [36] Soummer, R., “Apodized Pupil Lyot Coronagraphs for Arbitrary Telescope Apertures,” *Astrophysical Journal, Letters* **618**, L161–L164 (Jan. 2005).
- [37] Guerri, G., Daban, J.-B., Robbe-Dubois, S., Douet, R., Abe, L., Baudrand, J., Carbillet, M., Boccaletti, A., Bendjoya, P., Gouvret, C., and Vakili, F., “Apodized Lyot coronagraph for SPHERE/VLT: II. Laboratory tests and performance,” *Experimental Astronomy* **30**, 59–81 (May 2011).